

## Supplementary File

### **A mechanism of platelet integrin $\alpha$ IIb $\beta$ 3 outside-in signaling through a novel integrin $\alpha$ IIb subunit-filamin-actin linkage**

Jianmin Liu, Fan Lu, Sujay Subbayya Ithychanda, Marcin Apostol, Mitali Das, Gauravi Deshpande, Edward F Plow, and Jun Qin\*

**(Methods, 3 supplementary tables, and 5 supplementary figures)**

#### **Methods**

**Plasmid constructs, protein/peptide preparation, and NMR sample preparation** – For FLNa-Ig21- $\alpha$ IIb chimera protein, cDNAs of  $\alpha$ IIb CT was inserted into GST-FLNa-Ig21 plasmid construct at FLNa-Ig21's C-terminus using QuikChange Site-Directed Mutagenesis Kits. Spacer amino acids (GASGSGASGSSGS) were included between Ig21 and  $\alpha$ IIb CT as a linker to provide flexibility for binding between FLNa-Ig21 and  $\alpha$ IIb CT. cDNA of full-length human FLNa was cloned into pmCherry-C1 vector. F99A/L104E mutations were introduced using the QuikChange Site-Directed Mutagenesis Kit.

Human FLNa-Ig21 (2236-2330) and  $\alpha$ IIb CT (W988-E1008) were purified as previously described<sup>1</sup>. Unlabeled wide type  $\alpha$ IIb CT, and mutants  $\alpha$ IIb-N and  $\alpha$ IIb DDE to KKK were synthesized in Biotechnology core of Lerner Research Institute. All HSQC binding experiments used 0.05 mM or 0.1 mM <sup>15</sup>N-labeled proteins with or without the presence of certain ratio of binding partners. 5 mM PSPC vesicle with or without 20% PIP2 were used for HSQC experiment while 50 mM PSPC vesicle with 20% PIP2 was used for samples for the NMR structure

determination - 1 mM  $^{15}\text{N}/^{13}\text{C}$ -labeled or  $^{15}\text{N}/^2\text{D}$ -labeled FLNa-Ig21 with 1.2 mM  $\alpha\text{IIb}$  CT. Please see supplementary Table 3 for the information of primers used in cloning and mutagenesis.

**FRET Assay:** cDNAs of full length human  $\alpha\text{IIb}$ ,  $\beta 3$ , and FLNa Ig repeat 21 (G2236-G2330) were cloned into mTurquoise2-N1 (addgene #54843) and mVenus-N1 (addgene #27793), respectively.  $1.5 \times 10^5$  CHO-K1 cells (ATCC® CCL-61) were seeded on a microscope coverslips (d=18mm, Fisherbrand) within 12-well plates containing 1ml complete medium (DMEM:F12 supplemented with 10% fetal bovine serum). Cells were incubated under normal growth conditions (37 °C and 5% CO<sub>2</sub>) for overnight.  $\alpha\text{IIb}$ -mTur/ $\beta 3$ -mVen, or  $\alpha\text{IIb}$ -mTur/PC (pcDNA3.1)- $\beta 3$  (control), or PC- $\alpha\text{IIb}$ / $\beta 3$ -mTur (control), or PC- $\alpha\text{IIb}$ / $\beta 3$ -mTur/FLNa Ig21-mVen,  $\alpha\text{IIb}$ -mTur/PC- $\beta 3$ /FLNa Ig21-mVen was transfected using jetOPTIMUS transfection reagent (Polyplus) when overnight cell culture grew to 50-70% confluency. Transfected cells were maintained for another 24 hours. 200 nM PMA was added to cells (PMA groups) and incubated in cell culture incubator for 15 minutes. In order to overcome the low efficiency of FRET assays due to dynamic protein interactions, we fix cells before the FRET assay so cells were washed with PBS, fixed cells in 4% PFA at room temperature for 10 minutes and mounted on microscope slides (25x75mm, Fisherfinest) with Prolong Diamond Antifade mountant. The FRET assay was performed on Leica TCS-SP8 inverted confocal microscope equipped with LAS-X FRET module software (Leica Microsystems, GmbH, Wetzlar, Germany) using 63x oil (NA 1.32) objectives. Pinhole was set at maximum (6.78). Acceptor (mVenus) photobleaching was done in 10 frames using 488 nm laser, resulting in more than 90% reduction in the fluorescence intensity of mVenus without direct effect on mTurquoise emission intensity (checked by  $\alpha\text{IIb}$ -mTur/PC- $\beta 3$  and PC- $\alpha\text{IIb}$ / $\beta 3$ -mTur transfected CHO-K1 cells, data not shown). The photobleached area typically included one or two cells. Pre- and post-bleach

image sets of both donor (mTurquoise) and acceptor (mVenus) were acquired. Using Image pro plus 7.0 (Media Cybernetics, Inc., Rockville, Maryland, USA), mTurquoise signals in a ring outlining the cell membrane were selected as the region of interest and the intensities of pre- and post-bleached donor (mTurquoise) signal were counted.

FRET efficiency (E) was calculated as

$$E = 1 - (F_{mTur(d)Pre} / F_{mTur(d)Post})$$

where  $F_{mTur(d)Pre}$  and  $F_{mTur(d)Post}$  are the mTurquoise emission intensity prior to and following mVenus photobleaching.

**Preparation of PIP2 containing PSPC vesicle** – PSPC vesicles containing PS (L-alpha-phosphatidylserine) and PC (L-alpha-phosphatidylcholine). PS, PC, and PIP2 were all purchased from Avanti Polar Lipids (Alabaster, AL, USA). PSPC vesicles were prepared by mixing PS and PC in chloroform at 10:90 ratio. To prepare the PIP2 containing PSPC vesicles, lipids in chloroform were mixed in molar ratio of PS:PO:PIP2 = 10:70:20 for PIP2 inserted PSPC vesicles. The chloroform was removed under a stream of nitrogen followed by overnight vacuum pumping. The lipid film was re-hydrated in desired buffer. The lipid suspension was subjected to a few freeze-thaw cycles by a dry ice/alcohol bath and a room temperature shaker. The vesicles were formed by extruding the lipid suspension ~20 times through two stacked 0.1 um polycarbonate filters (Avanti Polar Lipids) using Avanti Mini Extruders.

**NMR experiment and Solution NMR structure determination** – All NMR experiments were performed on Bruker 600MHz, and 900MHz spectrometers, located in Cleveland Center for Membrane and Structural Biology, each equipped with a triple resonance probe. All experiments

were performed at 25°C in 25mM Sodium Phosphate, pH 6.4, 5mM NaCl, 1mM TCEP. Note that high salt condition yields the same NMR spectra whereas the low salt condition increases the solubility of the sample and minimizes the sample aggregation problem (Fig S5). Standard triple resonance experiments, as previously described<sup>2</sup>, were used for assigning <sup>13</sup>C-<sup>15</sup>N FLNa-Ig21 bound to unlabeled αIib-CT in 50mM 20% PIP2 inserted PSPC vesicle. 2D NOESY/TOCSY were used to assign αIib-CT bound to FLNa-Ig21 in 50mM 20% PIP2 inserted PSPC vesicle. Intermolecular NOEs were obtained from 3D <sup>15</sup>N-edited NOESY experiment (150 ms mixing time) using <sup>2</sup>D-<sup>15</sup>N FLNa-Ig21 bound to αIib-CT. 2D transferred NOESY experiment (400 ms mixing time) were run on 2 mM αIib-CT, or αIib-N, or αIib-CT DDE to KKK mutant in the presence of 0.05 mM MBP-β3 or GST-FLNa-Ig21. NMR data were processed by NMRPipe, and visualized and analyzed by SPARKY (T.D. Goddard and D.G. Kneller, SPARKY 3, University of California, San Francisco). X-plor-NIH was used for calculating the structure. Structure quality was evaluated using the program PROCHECK. The structure has been deposited in the Protein Data Bank under the accession code 7SFT.

**Surface Plasmon Resonance (SPR) experiment** – SPR experiment were conducted on the BIAcore 3000 system at the Molecular Biotechnology core of the Lerner Research Institute. The experiment was carried out at 25°C, using buffer, 25 mM Sodium Phosphate, PH 6.4, 5 mM NaCl, 1 mM TCEP, 0.1% BSA. αIib-N was immobilized on CM5 sensor chip for about 100 RU. FLNa-Ig21 was flowed over the chip surface. Kinetics were fitted using 1:1 Langmuir binding model in the BIAevaluation software, version 4.0.1.

**Crystallization and crystal structure determination** - Crystals were obtained by sitting drop vapor diffusion method at 16 °C. To set up a sitting drop, 1 ul of concentrated protein solution (10 mg/ml) was mixed with 1ul of crystallization solution with 2 M Ammonium Sulfate, 5% 2-propanol. Data were collected at the Advanced Photon Source (APS) beamline 19-ID in Argonne, Illinois. Data was collected at a wavelength of 0.97934 Å. Glycerol was used as a cryoprotectant and the crystals were cooled to -180°C during data collection. Data were collected using 1 degree wedges. Images were indexed and scaled using the program ‘HKL2000’<sup>3</sup>. Phases were calculated by the molecular replacement method utilizing the program ‘Phaser’<sup>4</sup>. Refinement was carried out with a TLS model using the program ‘REFMAC’<sup>5</sup>. Iterative model building was performed with the program ‘coot’<sup>6</sup>. Data collection and refinement statistics for both crystal forms are given in supplementary Table 1. The program ‘PROCHECK’ was used to check the Ramachandran statistics for the model<sup>7</sup>. The structure has been deposited in the Protein Data Bank under the accession code 7SC4. The structure is illustrated using the program ‘PyMol’<sup>8</sup>. Note that the protein crystallized is a chimera as mentioned in the text, in which the N-terminal tail of integrin  $\alpha$ IIB-CT was fused to FLNa-Ig21 with a flexible linker. The sequence of the crystallized construct is below:

GAMDPGGAHKVVRAGGPGLERAEAGVPAEFSIWTREAGAGGLAIAVEGPSKAEISFEDRKDGS  
CGVAYVVQEPGDYEVSVKFNEEHIPDSPFVVPVASPSGGASGSGASGSSGSWKVGFVKRNRP  
PLEEDDEEGE

Two chimeras are found within the asymmetric unit of the crystal. Highlighted in blue, green and orange are residues which can be resolved in the electron density map. The blue are residues 2236-2329 of FLNa-Ig21. The orange residues are 988-999 of integrin  $\alpha$ IIB-CT. In green are residues from the connecting linker.

**Flow cytometry** - About 80% confluent CHO-A5 cells ( $\alpha$ IIB $\beta$ 3 integrin stably expressing cell line) were transfected with desired plasmid DNAs using JetOPTIMUS transfection reagent

(Polyplus) and further grown for 24 hours. Cells were harvested with non-enzyme disassociation solution (Corning) and were resuspended at  $1 \times 10^7$  cells per ml in HBSS plus 5% BSA. Cells were centrifuged at 500xg for 5 minutes after washing and stained with PAC-1 primary antibody (BD Biosciences, #340535) for 30 minutes at room temperature. Cells were washed and centrifuged, and then fixed in 2% paraformaldehyde (PFA) in phosphate-buffered saline for 10 minutes at room temperature. Cells were washed/centrifuged and stained with the Alexa647 secondary antibody (Thomas Scientific, # C840X46) for 30 minutes at 4°C. Cells were washed/centrifuged and resuspended in 200ul HBSS+BSA buffer. Cells was analyzed by LSRFortessa Cell Analyzer (BD) in Cleveland Clinic Lerner Research Institute Flow Cytometry core.

**Immunostaining and focal adhesion analysis** –Overnight transfected mouse embryonic fibroblasts were trypsinized and seeded onto fibronectin coated coverslips to allow adhesion and spreading in 37°C incubator for 30min or 1h. After incubation, cells were fixed with 4% formaldehyde at room temperature for 15min, followed by permeabilization with 0.1% Triton X-100. After permeabilization, cells were blocked with 5% goat serum for 30min and stained with anti-GFP (abcam #ab13970) and anti-vinculin (EMD millipore #MAB3574-C) overnight at 4°C. After several washes, coverslips were incubated with anti-chicken Alexa488 (abcam #ab150173), anti-mouse Alexa568 (Invitrogen #A-11004) and phalloidin-Alexa647 (Invitrogen A22287) at room temperature for 30 min and mounted onto the slides with Prolong Diamond Antifade Mountant with DAPI for 24h. Images were acquired by using upright Leica SP5 confocal microscope equipped with 63x oil lens and Leica confocal software (LAS-AF). All images were processed in LAS X software (and subject to analysis in ImageJ). Filamin expression was

examined by anti-human filamin antibody (Sigma #MAB1678) meanwhile GAPDH (#5174, Cell Signaling Technology) serving as loading control.

**Wound healing** – About 80% confluent HEK293T cells (ATCC® CRL-3216) were transfected with FLNa or FLNa F99A/L104E plasmid using JetOPTIMUS transfection reagent (Polyplus) and further grown for 24 hours. A scratch was introduced with a 20ul pipette tip. Cells were washed with PBS to remove cell debris and fresh medium was added with or without 200 nM PMA. Scratches were imaged at time 0 hour and 24 hours with inverted fluorescence microscope (Olympus CKX53) with a 20x objective using the operation software of infinity 3S lumenera. Images were analyzed by ImageJ.

**Human platelet spreading and immunoprecipitation** – All experiments done with human platelets were approved by the Cleveland Clinic's Institutional Review Committee. Platelets were isolated as described previously<sup>9</sup>. The platelet pellet was re-suspended in Tyrode's buffer (with no EDTA) and counted using a hemocytometer. 1 ml of  $2 \times 10^7$  cells/ml platelets were seeded on coverslips pre-coated with 20  $\mu$ g/ml fibrinogen and allowed to spread for 30min, 60min, 90min, and 120min. At 0 min, 1 ml of  $4 \times 10^6$  cells/ml platelets were seeded on precoated coverslips and centrifuged at 1500 RPM for 3 minutes without brake. After buffer removed, platelets were washed, fixed, permeabilized, blocked with goat serum, then incubated with anti- $\beta$ 3 (Kerafast #EBW106), anti-filamin A (Cell Signaling #4762) primary antibodies at 4 °C for overnight. After three washes, platelets were incubated with Alexa Fluor 488 (Abcam #ab150117) and 568 (Abcam #ab175696) secondary antibodies at room temperature for 30 minutes. After three washes, platelets were incubated with anti-talin-1 antibody conjugated with Alexa Fluor 647 (Santa Cruz #sc-

365875 AF647) at 4 °C for overnight. After three washes, platelets were sealed with anti-fade mountant (Invitrogen #P36930). Confocal images were taken at 100x/1.49 NA oil immersion lens of an inverted Leica SP8 confocal microscope.

1 ml of  $2 \times 10^8$  cells/ml platelets were stimulated by 0.5 mM  $\text{MnCl}_2$  and lysed on ice by the addition of 5 x Ripa lysis buffer (with no EDTA) with freshly added protease and phosphatase inhibitors. Note that we chose  $\text{Mn}^{2+}$  over natural platelet agonists such as thrombin or ADP because thrombin or ADP is known to stimulate GPCRs to activate integrins whereas GPCRs also bind to filamin<sup>10</sup> therefore causing complication of Co-IP since GPCR and integrin may compete for the same pool of filamin in the cell for binding. By contrast,  $\text{Mn}^{2+}$  specifically and directly stimulates integrin, therefore avoiding the complication problem. The total protein concentration in lysates were measured by Pierce BCA protein assay kit (Fisher #23227). Lysates containing 1 mg total protein were precleared with protein A/G agarose (Santa Cruz #sc-2003) and 1 ug mouse IgG (Santa Cruz #sc-2025), then immunoprecipitated by using 5 ul per sample of anti- $\beta_3$  antibodies (1:1 mixture of Santa Cruz #sc-21783 and Kerfast #EBW106) at 4 °C for overnight. Lysates were treated by protein A/G agarose at 4 °C for 2 hours. After 4 washes with 1 x Ripa lysis buffer, agaroses were eluted with 4 x loading buffer and analyzed by primary and secondary antibodies.

**Analysis of  $\alpha\text{IIb}\beta_3$  outside-in signaling in HEL cells** – HEL cells were transfected using nucleofection kit V from Lonza, according to the manufacturer instructions and program X-005. Post nucleofection, cells were incubated for overnight and then serum-starved for 12 hours. Cells were stimulated by 0.5 mM  $\text{MnCl}_2$  in the presence of 25  $\mu\text{g}/\text{mL}$  fibrinogen in suspension for 0 or 5 minutes, pelleted, and lysed on ice by the addition of Ripa lysis buffer (with no EDTA) with freshly added protease and phosphatase inhibitors. The total protein concentration in lysates were



measured by Pierce BCA protein assay kit (Fisher #23227). Equal amount of total proteins were loaded onto SDS gel and analyzed by antibodies of anti-phosphorylated SRC Tyr416 (Cell signaling, #2101), anti-phosphorylated FAK Tyr397 (Cell signaling, #3283), anti-SRC (Cell signaling, #2109), anti-FAK (Cell signaling, #2712), anti-GFP (Cell signaling, #2956).

## References

1. Liu J, Das M, Yang J, et al. Structural mechanism of integrin inactivation by filamin. *Nat Struct Mol Biol.* May 2015;22(5):383-9. doi:10.1038/nsmb.2999
2. Zhou Y, Hu M, Chen X, et al. Migfilin supports hemostasis and thrombosis through regulating platelet alphaIIb beta3 outside-in signaling. *Haematologica.* Nov 1 2020;105(11):2608-2618. doi:10.3324/haematol.2019.232488
3. Otwinowski Z, Minor W. Processing of X-ray diffraction data collected in oscillation mode. *Methods Enzymol.* 1997;276:307-26.
4. McCoy AJ, Grosse-Kunstleve RW, Adams PD, Winn MD, Storoni LC, Read RJ. Phaser crystallographic software. *J Appl Crystallogr.* Aug 1 2007;40(Pt 4):658-674. doi:10.1107/S0021889807021206
5. Murshudov GN, Vagin AA, Dodson EJ. Refinement of macromolecular structures by the maximum-likelihood method. *Acta Crystallogr D Biol Crystallogr.* May 1 1997;53(Pt 3):240-55. doi:10.1107/S0907444996012255
6. Emsley P, Lohkamp B, Scott WG, Cowtan K. Features and development of Coot. *Acta Crystallogr D Biol Crystallogr.* Apr 2010;66(Pt 4):486-501. doi:10.1107/S0907444910007493
7. Laskowski RA, MacArthur MW, Moss DS, Thornton JM. PROCHECK: a program to check the stereochemical quality of protein structures. *Journal of Applied Crystallography.* 1993;26(2):283-291. doi:doi:10.1107/S0021889892009944
8. Schrodinger, LLC. The PyMOL Molecular Graphics System, Version 1.8. 2015.
9. Bialkowska K, Byzova TV, Plow EF. Site-specific phosphorylation of kindlin-3 protein regulates its capacity to control cellular responses mediated by integrin alphaIIb beta3. *J Biol Chem.* Mar 6 2015;290(10):6226-42. doi:10.1074/jbc.M114.634436
10. Tirupula KC, Ithychanda SS, Mohan ML, Naga Prasad SV, Qin J, Karnik SS. G protein-coupled receptors directly bind filamin A with high affinity and promote filamin phosphorylation. *Biochemistry.* Nov 10 2015;54(44):6673-83. doi:10.1021/acs.biochem.5b00975

**Supplementary Table 1.** Crystallographic statistics of FLNa-Ig21/ $\alpha$ IIb-CT (7SC4)

Apo Crystal	
<b>Data Collection</b>	
Spacegroup	P2 <sub>1</sub> 2 <sub>1</sub> 2 <sub>1</sub>
Cell dimensions: a,b,c (Å)	50.25, 66.01, 71.89
Wavelength (Å)	0.97934
Resolution (Å)	100-1.85 (1.88-1.85)
R <sub>merge</sub>	0.050 (0.638)
I / $\sigma$ I	38.8 (3.0)
Completeness (%)	99.9 (100.0)
Redundancy	5.9 (5.8)
<b>Refinement</b>	
Resolution (Å)	34.94-1.849
No. reflections	21100
R <sub>work</sub> / R <sub>free</sub>	0.199 / 0.268
No. atoms	
Protein	1678
Ligand/ion	5
Water	110
<i>B</i> -factors	
Protein	35.01
Ligand/ion	64.59
Water	40.16
R.m.s deviations	
Bond lengths (Å)	0.020
Bond angles (°)	1.757
Ramachandran plot	
Most favored regions (%)	88.9
Additionally allowed regions (%)	11.1
Generously allowed and Disallowed regions (%)	0.0

**Supplementary Table 2.** Solution NMR statistics of FLNa-Ig21/ $\alpha$ IIb-CT in 20% PIP2 inserted PSPC vesicle (7SFT)

Parameter	SA Ensemble <sup>a</sup>
Rmsd from experimental distance restraints (Å)	
Total intramolecular (858)	0.03670 ± 0.00287
Intraresidue, $i = j$ (457)	0.03090 ± 0.00544
Sequential, $ i - j  = 1$ (206)	0.03610 ± 0.00337
Medium range, $ i - j  < 5$ (47)	0.04990 ± 0.00435
Long range, $ i - j  \geq 5$ (147)	0.04740 ± 0.00351
Intermolecular (21)	0.04660 ± 0.01358
Rmsd from idealized covalent geometry	
Bonds (Å)	0.00518 ± 0.00007
Angles (°)	0.73324 ± 0.01041
Impropers (°)	1.72257 ± 0.01387
E <sub>LJ</sub> (kcal/mol) <sup>b</sup>	-388.199 ± 10.175
Ramachandran plot <sup>c</sup>	
Most favored regions (%)	67.2
Additionally and generously allowed regions (%)	32.6
Disallowed regions (%)	0.1
Coordinate precision <sup>d</sup>	
Rmsd of backbone atoms to the mean (Å)	0.557 ± 0.083
Rmsd of all heavy atoms to the mean (Å)	1.119 ± 0.114
<sup>a</sup> Mean ± standard error where applicable	
<sup>b</sup> Lennard-Jones potential energy function, calculated with CHARMM19 empirical energy parameters	
<sup>c</sup> Residues FLNa-Ig21(2239-2330)/ $\alpha$ IIb-CT(988-996)	
<sup>d</sup> Residues FLNa-Ig21(2239-2330)/ $\alpha$ IIb-CT(988-996)	

**Supplementary Table 3.** Primer sequence information

Plasmid Construct	Primer sequence (5' – 3')
Filamin A Ig-21 - mVenus	Destination Vector Forward: GTGAGCAAGGGCGAGGAGC Destination Vector Reverse: CATGGTGGCGACCGGTGG Insert Forward: CCGGTCGCCACCATGGGGGGAGCCCACAAGGTC Insert Reverse: CTCGCCCTTGCTCACGCCAGACGGAGAAGCCAC
Integrin $\beta$ 3 - mVenus	Destination Vector Forward: GTGAGCAAGGGCGAGGAGC Destination Vector Reverse: CATGGTGGCGACCGGTGG Insert Forward: CCGGTCGCCACCATGGGGCGAGCGCGGCCGCGG Insert Reverse: CTCGCCCTTGCTCACAGTGCCCCGGTACGTGATATTGG
Integrin $\alpha$ IIb - mTurquoise	Destination Vector Forward: GTGAGCAAGGGCGAGGAG Destination Vector Reverse: CATGGTGGCGACCGGTAG Insert Forward: CCGGTCGCCACCATGGCCAGAGCTTTGTGTCCACTG Insert Reverse: CTCGCCCTTGCTCACCTCCCCCTCTTCATCATCTTCTTCC
Filamin A Ig-21 – $\alpha$ IIb CT Chimeric	Forward: GCCTGTGGCTTCTCCGTCTGGCGGCGCTTCTGGCTCTGGCGCTTCTGGCTCTtggagggtcggcttctcaagc Reverse: CGAGACTGCAGGCTCTAGACTACTCCCCCTCTTCATCATCTTC
pmCherry-C1-Filamin A full-length	Oligo 1 (HindIII) (Insert 1) Forward TCTCGAGCTCAAGCTTCGATGAGTAGCTCCCACTCTCG Oligo 2 (Insert 1) (BamHI) Reverse TAGATCCGGTGGATCCTCAGGGCACCACAACGCG
Filamin A actin-deficient mutation F99A/L104E	Forward: CCAGCGGCCCACTGCCCGCCAAATGCAGGAAGAGAACGTGTCCG Reverse: CCGACACGTTCTCTTCCTGCATTTGGCGGGCAGTGGGCCGCTGG

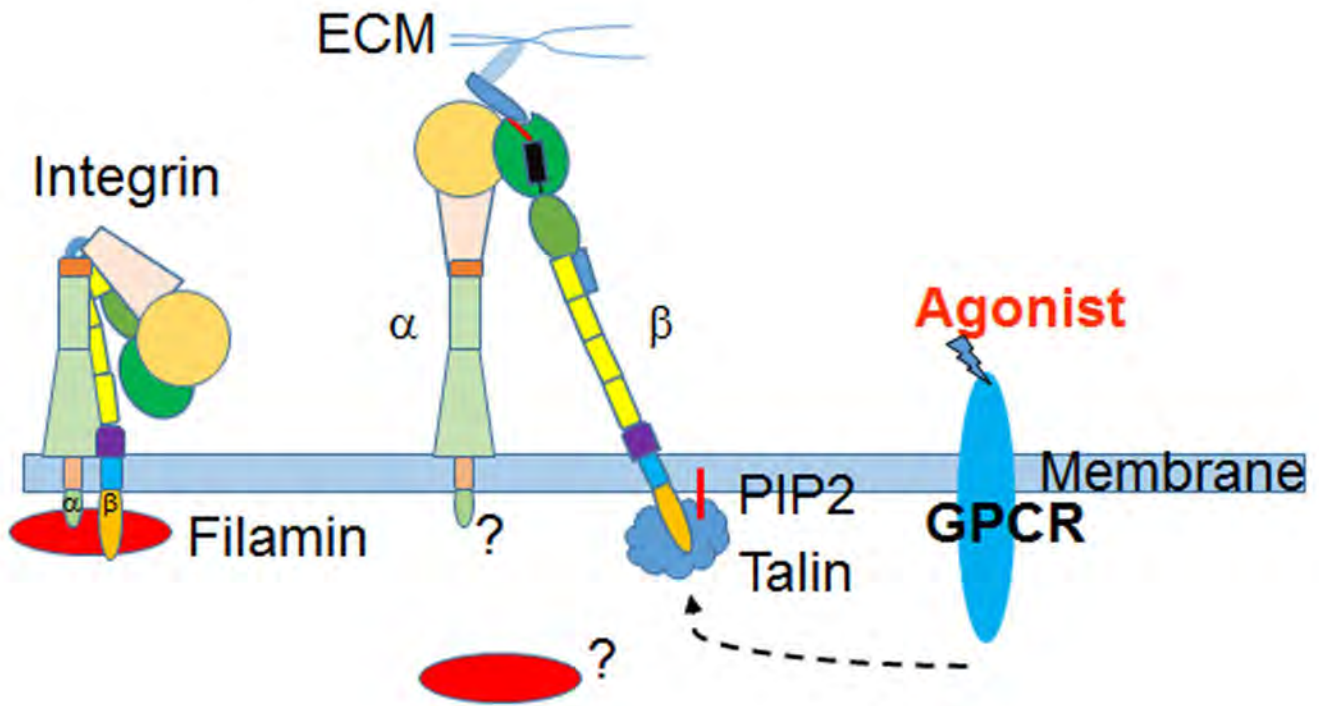


**Figure S1.** The current dogma of the integrin activation. Please see details in text. Question marks on integrin  $\alpha$  CT and filamin indicate that their roles after integrin activation are unrevealed.

$\alpha$ IIb-mTur/ $\beta$ 3-mVen

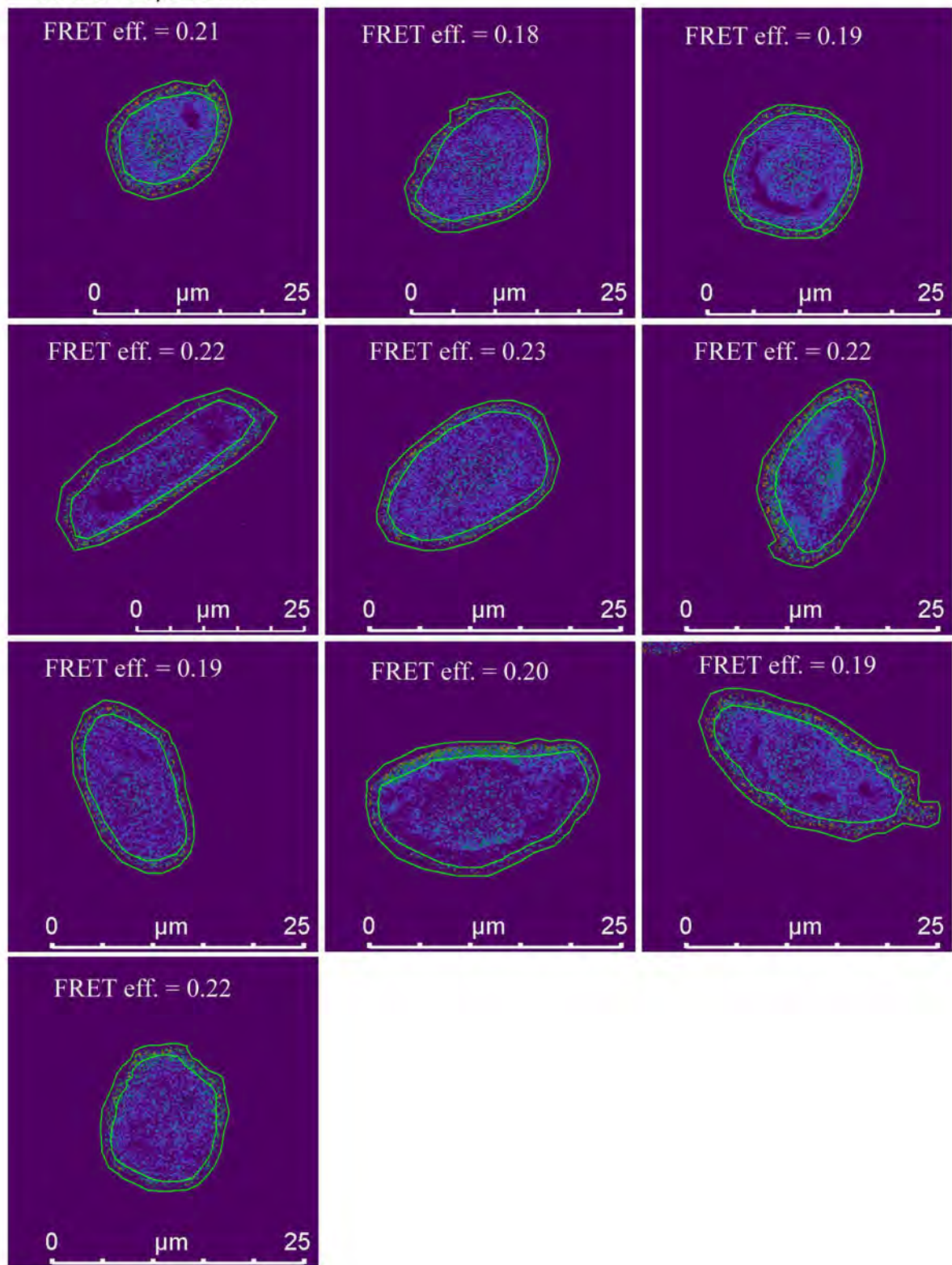


**Figure S2.** Images of Fluorescence Resonance Energy Transfer (FRET) efficiency by acceptor (mVenus) photobleaching of mTurquoise-mVenus pair that was transfected in CHO-K1 cells. Rings outlining the cell membrane were selected as the region of interest (ROI). Ten cells in each group were analyzed. **(A)**  $\alpha$ IIb-mTur/ $\beta$ 3-Ven pair without PMA treatment.

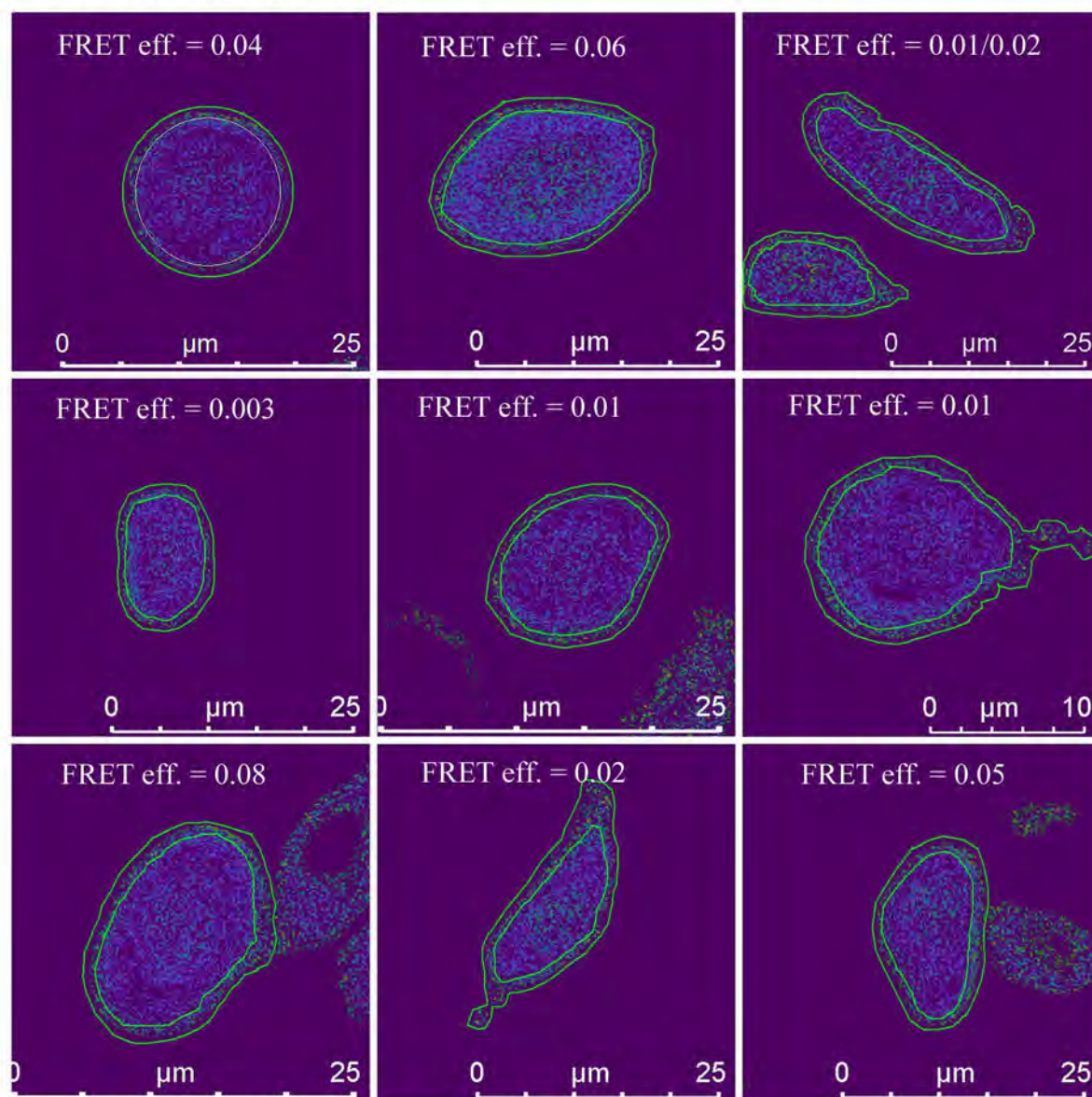


**Figure S2.** Images of Fluorescence Resonance Energy Transfer (FRET) efficiency by acceptor (mVenus) photobleaching of mTurquoise-mVenus pair that was transfected in CHO-K1 cells. Rings outlining the cell membrane were selected as the region of interest (ROI). Ten cells in each group were analyzed. **(B)**  $\alpha$ IIb-mTur/ $\beta$ 3-Ven pair with PMA treatment.

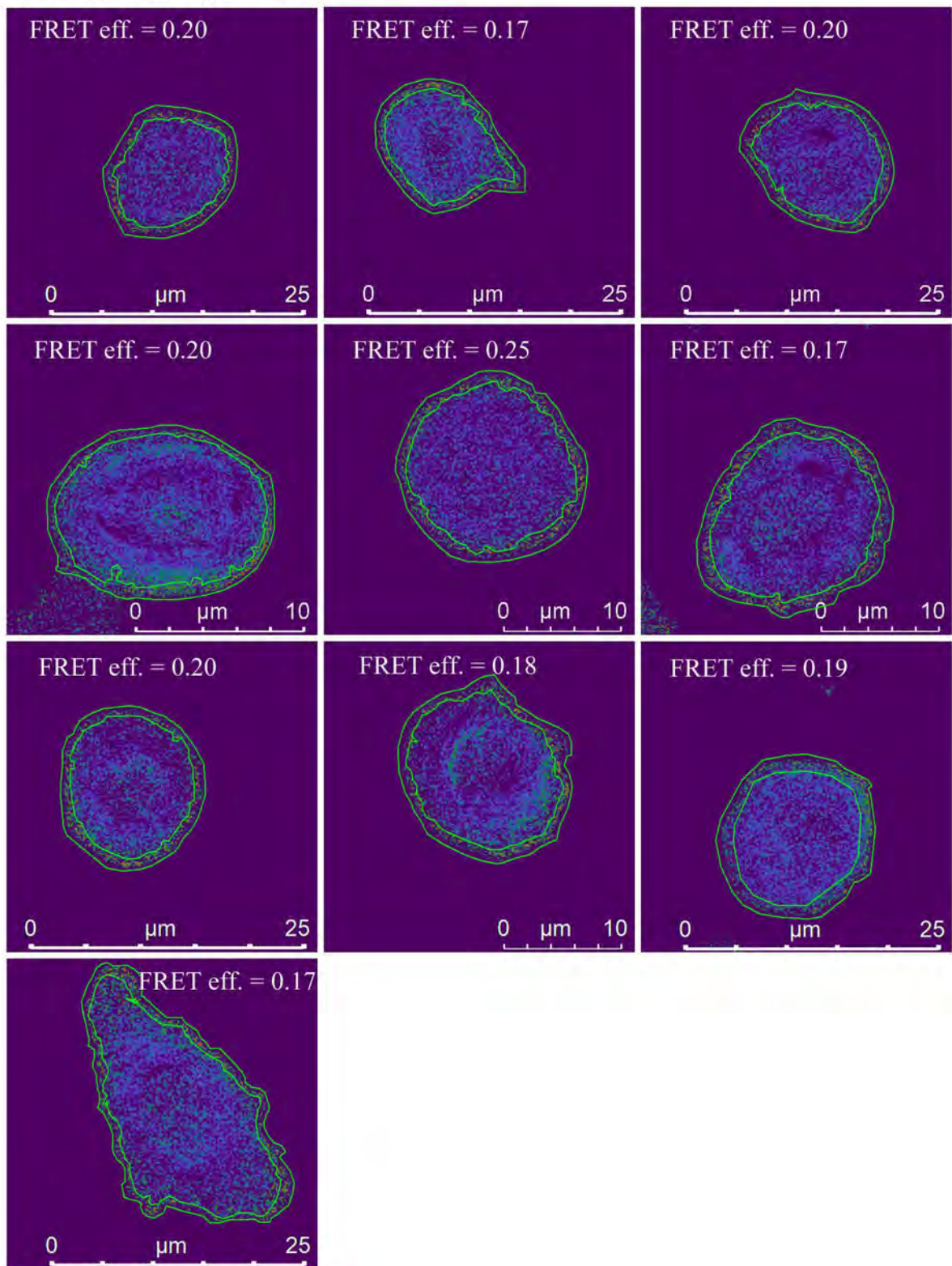


**Figure S2.** Images of Fluorescence Resonance Energy Transfer (FRET) efficiency by acceptor (mVenus) photobleaching of mTurquoise-mVenus pair that was transfected in CHO-K1 cells. Rings outlining the cell membrane were selected as the region of interest (ROI). Ten cells in each group were analyzed. **(C)**  $\beta$ 3-mTur/FLNa Ig21-mVen pair without PMA treatment.



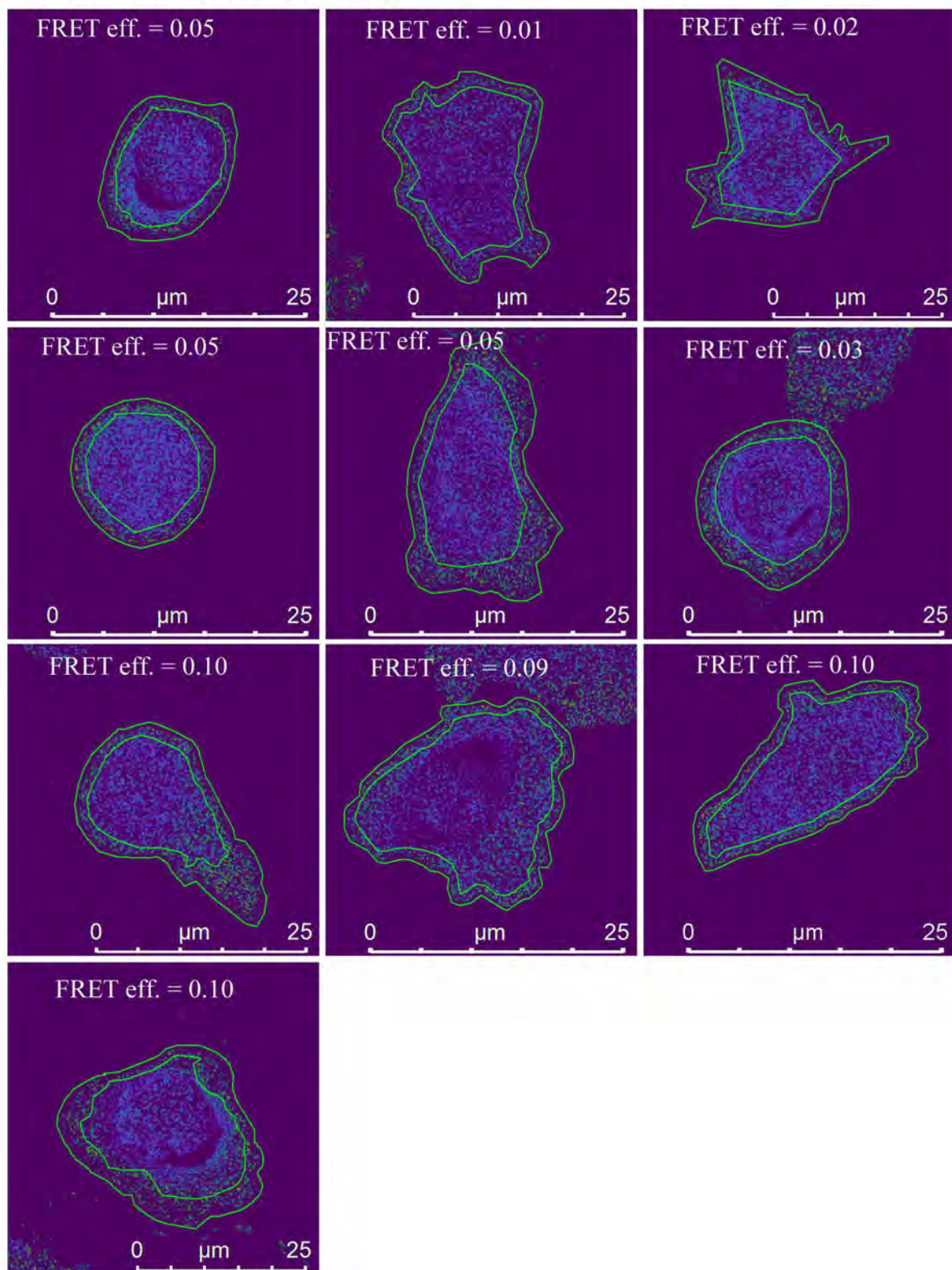


**Figure S2.** Images of Fluorescence Resonance Energy Transfer (FRET) efficiency by acceptor (mVenus) photobleaching of mTurquoise-mVenus pair that was transfected in CHO-K1 cells. Rings outlining the cell membrane were selected as the region of interest (ROI). Ten cells in each group were analyzed. **(D)**  $\beta$ 3-mTur/FLNa Ig21-mVen pair with PMA treatment.

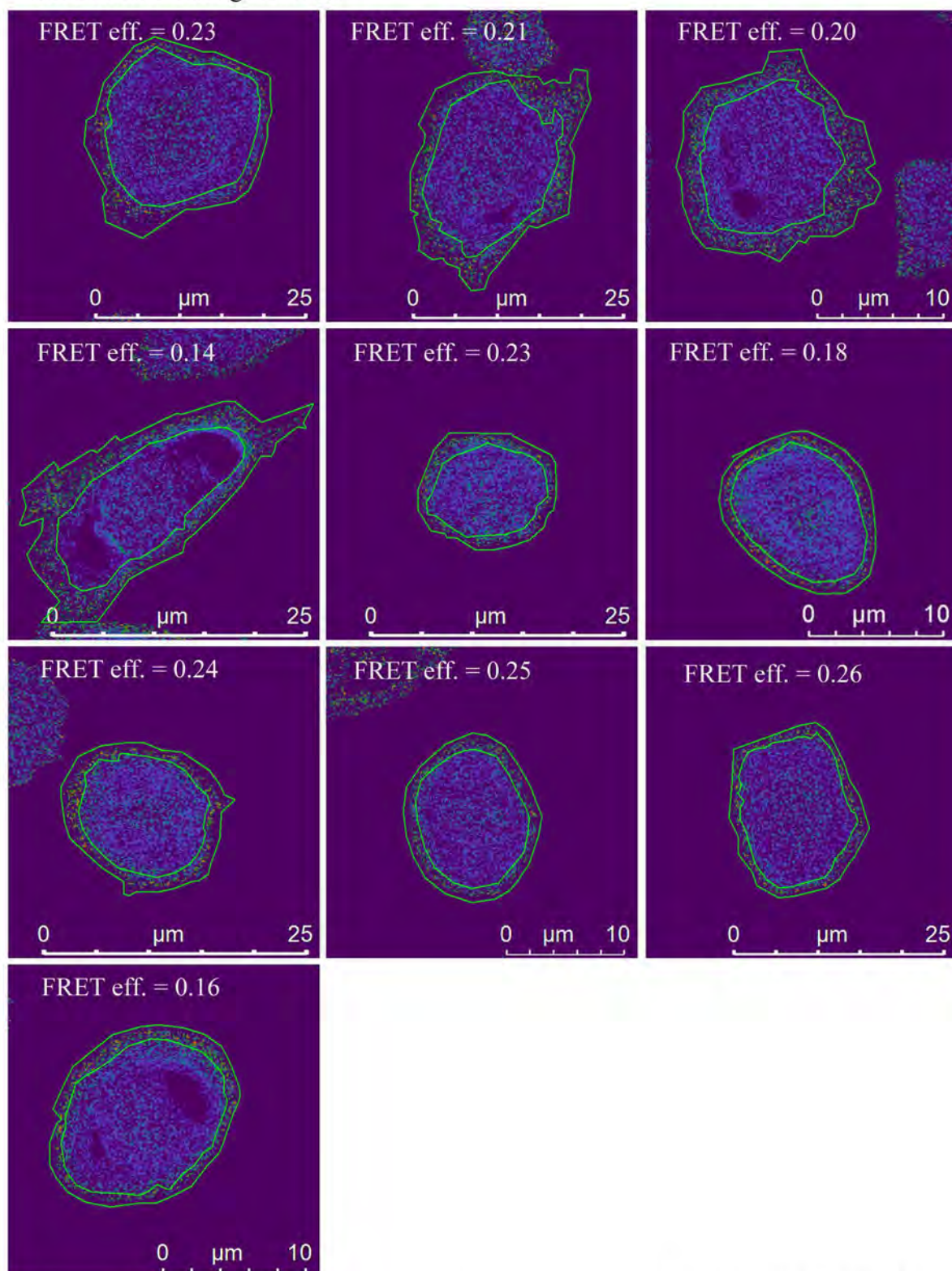


**Figure S2.** Images of Fluorescence Resonance Energy Transfer (FRET) efficiency by acceptor (mVenus) photobleaching of mTurquoise-mVenus pair that was transfected in CHO-K1 cells. Rings outlining the cell membrane were selected as the region of interest (ROI). Ten cells in each group were analyzed. **(E)**  $\alpha$ IIb-mTur/FLNa Ig21-mVen pair without PMA treatment.

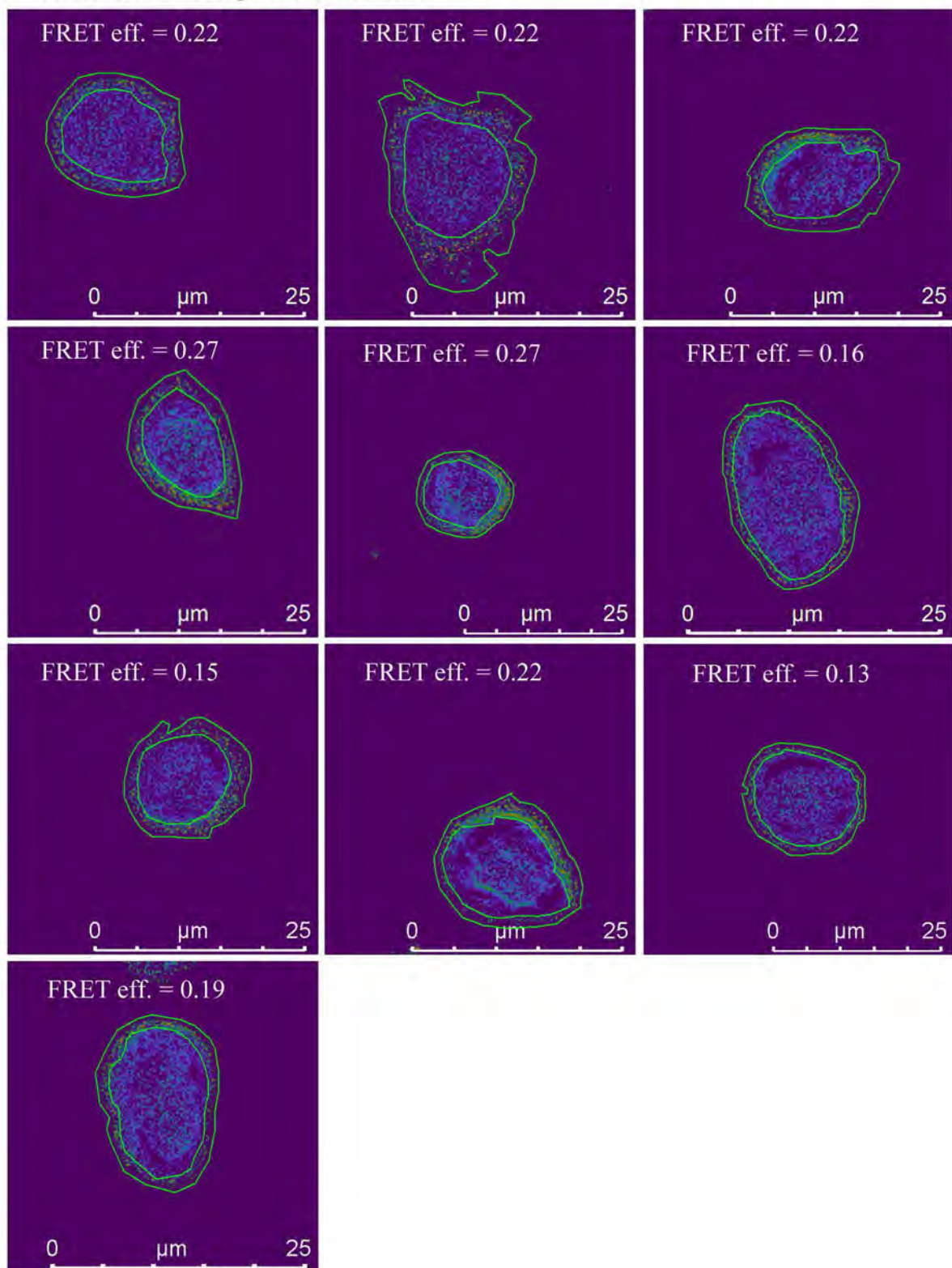


**Figure S2.** Images of Fluorescence Resonance Energy Transfer (FRET) efficiency by acceptor (mVenus) photobleaching of mTurquoise-mVenus pair that was transfected in CHO-K1 cells. Rings outlining the cell membrane were selected as the region of interest (ROI). Ten cells in each group were analyzed. **(F)**  $\alpha$ IIb-mTur/FLNa Ig21-mVen pair with PMA treatment.

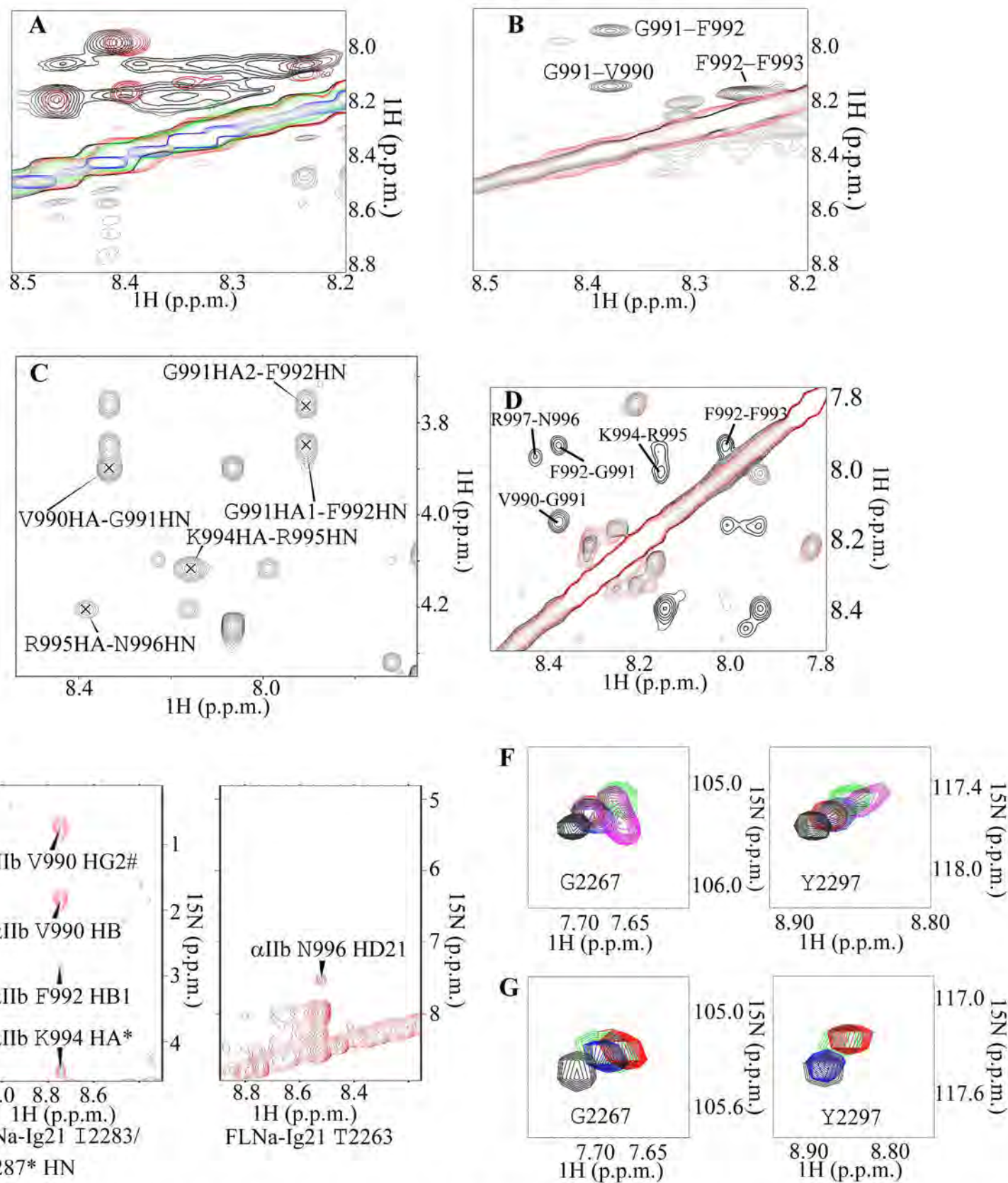


**Figure S3.** (A) Selected region of 2D transferred NOESY of 2 mM  $\alpha$ I**Ib**-N in the absence (black) and presence (red) of 0.05 mM MBP- $\beta$ 3 CT or presence (green) of 0.05 FLNa-Ig21 or presence (blue) of 0.05 mM GST-FLNa-Ig21. Residue labels are marked on the spectrum of  $\alpha$ I**Ib**-N with MBP- $\beta$ 3. (B) Selected region of 2D transferred NOESY of 2 mM  $\alpha$ I**Ib** CT (black) or  $\alpha$ I**Ib** CT DDE to KKK (red) in the presence of 0.05 GST-FLNa-Ig21. (C) Strong sequential  $\alpha$ Hi-NHi+1 NOEs for  $\alpha$ I**Ib**-N bound to GST-FLNa-Ig21 suggesting the  $\beta$  strand conformation. (D) Selected region of 2D transferred NOESY of 2 mM  $\alpha$ I**Ib** CT in 0% PIP2 vesicle (black) or 20% PIP2 vesicle (red) in the presence of 0.05 mM GST-FLNa-Ig21. (E) Representative intermolecular NOE cross peaks used to determine the NMR solution complex structure of  $\alpha$ I**Ib** CT and FLNa-Ig21 in PIP2-inserted PSC vesicles. (F) Selected region of HSQC of 0.1 mM  $^{15}$ N-labeled FLNa-Ig21 in the absence (black) and presence (red) of 0.2 mM  $\alpha$ I**Ib** CT, or presence (green) of 0.2 mM  $\alpha$ I**Ib** CT and 0.2 mM  $\beta$ 3 CT, or presence (blue) of 0.2 mM  $\alpha$ I**Ib** CT and 0.2 mM  $\beta$ 3 CT and 0.3 mM Talin F2F3, or in 20% PIP2 vesicle and presence (magenta) of 0.2 mM  $\alpha$ I**Ib** CT and 0.2 mM  $\beta$ 3 CT and 0.3 mM Talin F2F3. (G) Control experiment of (F) without  $\alpha$ I**Ib** CT. Selected region of HSQC of 0.1 mM  $^{15}$ N-labeled FLNa-Ig21 in the absence (black) and presence (red) of 0.1 mM  $\beta$ 3 CT, or presence (green) of 0.1 mM  $\beta$ 3 CT and 0.2 mM Talin F2F3, or presence (blue) of 0.1 mM  $\beta$ 3 CT and 0.5 mM Talin F2F3. Text interpretation for (F): Unlabeled  $\alpha$ I**Ib** CT and  $\beta$ 3 CT were sequentially titrated into  $^{15}$ N-labeled FLNa-Ig21, which revealed sequential chemical shift changes of FLNa-Ig21 (peaks shifted from black to red, then further to green), indicating the ternary complex formation characteristic of the resting state of integrin as consistent with previous studies<sup>1</sup>; Then talin was added into the mixture of  $\alpha$ I**Ib**-CT/ $\beta$ 3-CT/FLNa-Ig21, which shows that talin was able to reverse the chemical shift changes (green peaks shifted towards black or blue) indicating that talin competes with FLNa-Ig21 for binding to integrin  $\beta$ 3 CT (see also the control experiment in (G)). As expected, some residual chemical shift changes remain due to the weak binding of  $\alpha$ I**Ib** CT with FLNa-Ig21 (blue peaks were not overlaid with black peaks); Next, the solution mixture of  $\alpha$ I**Ib** CT/ $\beta$ 3 CT/FLNa-Ig21/talin were transferred into PIP2-enriched PSC membrane vesicle to simulate the integrin activating membrane environment, showing substantial chemical shift changes (blue peaks shifted to magenta, significantly more than those of isolated  $\alpha$ I**Ib** CT binding to FLNa-Ig21 in solution (red peaks)), which is consistent with the drastic affinity change of the PIP2-driven FLNa-Ig21 binding to activated  $\alpha$ I**Ib** CT that underwent  $\alpha$  helix to  $\beta$  strand transition. Text interpretation for (G): Unlabeled  $\beta$ 3 CT were titrated into  $^{15}$ N-labeled FLNa-Ig21 (peaks shifted from black to red), indicating the complex formation; Then talin was added into the mixture of  $\beta$ 3-CT/FLNa-Ig21 at two different concentration (2x and 5x molar excess to  $\beta$ 3-CT), which shows that talin was able to reverse the chemical shift changes (red peaks shifted to green, further to blue, almost back to black) indicating that talin competes with FLNa-Ig21 for binding to integrin  $\beta$ 3 CT.

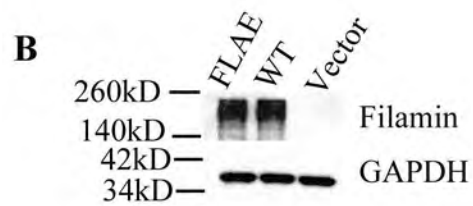
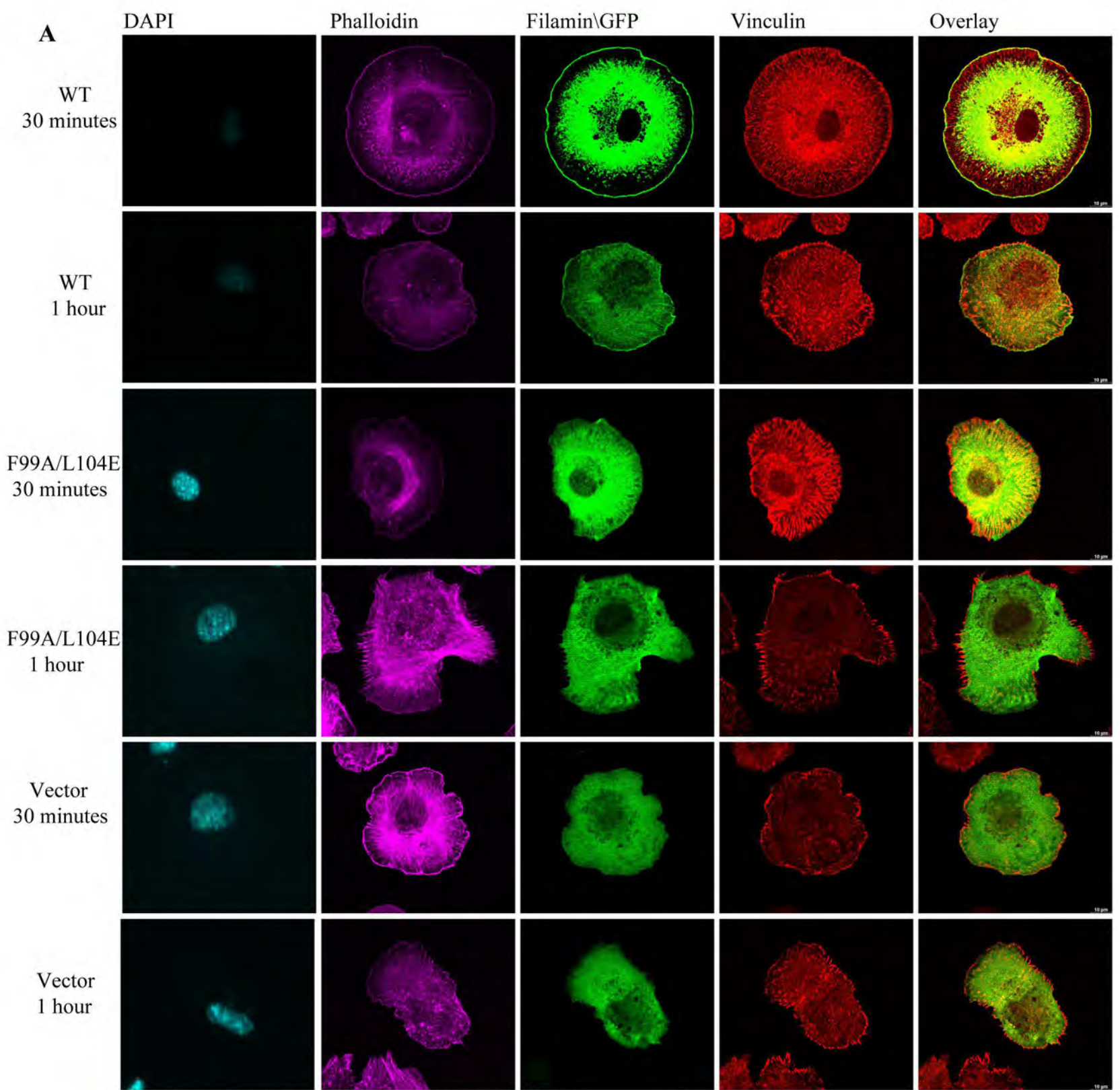
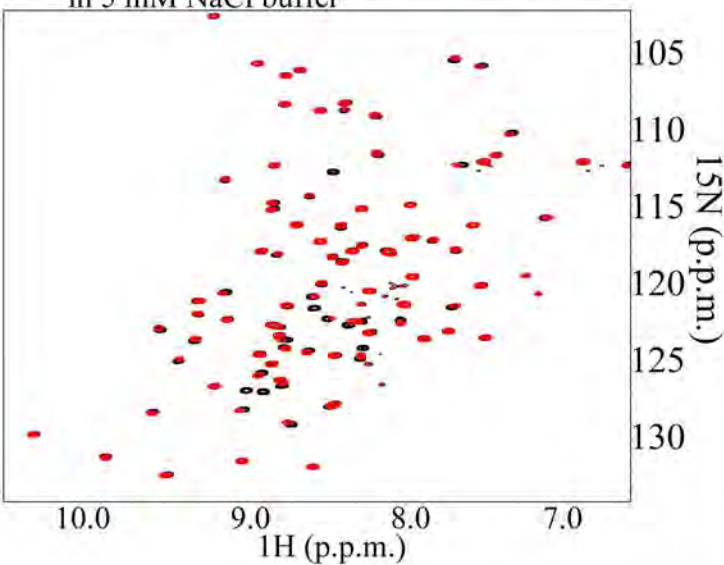


**Figure S4. (A)** Individual confocal sections of EGFP-filamin WT, F99A/L104E mutant, and EGFP alone in MEF cells fixed after plating on FN-coated glass slides for 30 minutes or 1 hour, and then stained for EGFP, Vinculin, and phalloidin. GFP-expressing cells were considered as filamin-expressing cells and therefore selected for images. Overlay is EGFP-filamin (green) and vinculin (red). **(B)** Western blot showing no expression variation between wide-type filamin and the filamin mutant. Please note that anti-human filamin antibody does not detect endogenous mouse filamin in MEF.

(A) Interaction of FLNa Ig21 and  $\alpha$ IIb CT (1:2)  
in 5 mM NaCl buffer



(B) Interaction of FLNa Ig21 and  $\alpha$ IIb CT (1:2)  
in 100 mM NaCl buffer

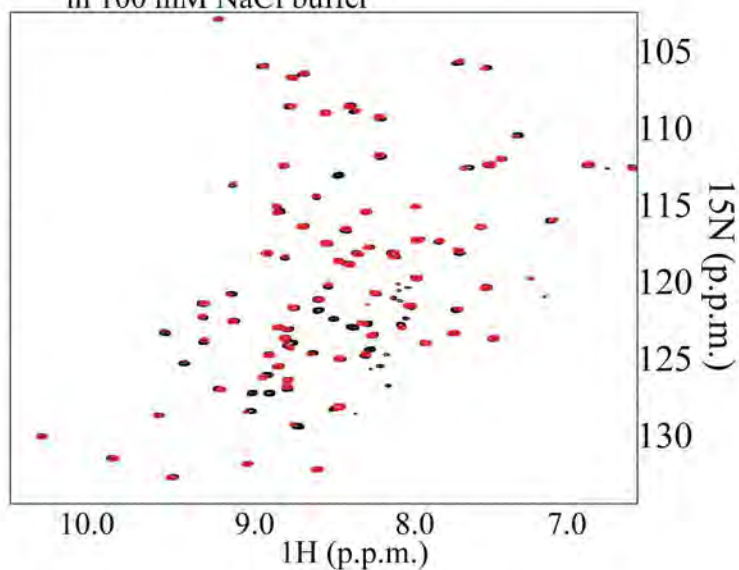


**Fig S5.** NMR spectra of 0.1 mM  $^{15}\text{N}$ -labeled FLNa-Ig21 in the absence (black) and presence (red) of 0.2 mM  $\alpha$ IIb CT at the low salt (A), 25 mM Sodium Phosphate, pH 6.4, 5 mM NaCl, 1 mM TCEP or the high salt (B), 25 mM Sodium Phosphate, pH 6.4, 100 mM NaCl, 1 mM TCEP conditions show the same binding mode. Note some more line-broadening occurs for the high salt sample probably due to some precipitation induced by the high salt.